ACS Macro Letters

Letter

Cite This: ACS Macro Lett. 2019, 8, 466−472

pubs.acs.org/macroletters

Predicting Monomers for Use in Aqueous Ring-Opening Metathesis Polymerization-Induced Self-Assembly

Spyridon Varlas,[†] Jeffrey C. Foster,[†] Lucy A. Arkinstall,[†] Joseph R. Jones,[†] Robert Keogh,[†,‡] Robert T. Mathers,[*,§] and Rachel K. O'Reilly[*,†]

[†]School of Chemistry, University of Birmingham, Edgbaston, Birmingham B15 2TT, U.K.

[‡]Department of Chemistry, University of Warwick, Gibbet Hill Road, Coventry CV4 7AL, U.K.

[§]Department of Chemistry, Pennsylvania State University, New Kensington, Pennsylvania 15068, United States

Supporting Information

ABSTRACT: Aqueous polymerization-induced self-assembly (PISA) is a well-established methodology enabling *in situ* synthesis of polymeric nanoparticles of controllable morphology. Notably, PISA *via* ring-opening metathesis polymerization (ROMPISA) is an emerging technology for block copolymer self-assembly, mainly due to its high versatility and robustness. However, a limited number of monomers suitable for core-forming blocks in aqueous ROMPISA have been reported to date. In this work, we identified seven monomers for use as either corona- or core-forming blocks during aqueous ROMPISA by *in silico* calculation of relative hydrophobicity for corresponding oligomeric models. The predicted monomers were validated experimentally by conducting ROMPISA using our previously reported two-step approach. In addition to predictive data, our computational model was exploited to identify trends between polymer hydrophobicity and the morphology of the self-assembled nano-objects they formed. We expect that this methodology will greatly expand the scope of aqueous ROMPISA, as monomers can be easily identified based on the structure−property relationships observed herein.

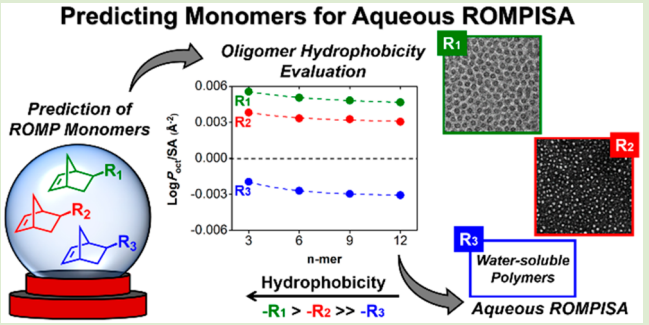

Conventional preparative methodologies for solution self-assembly of block copolymers have been extensively applied in modern polymer science.[1−4] These involve the synthesis of a block copolymer in organic solvent and multiple steps for its transition into a selective solvent for one or more blocks to allow for the formation of nanostructures. In general, such strategies are often limited by low polymer concentration (≤1% w/w) and precise morphology control issues.[5,6] Recently, polymerization-induced self-assembly (PISA) has been introduced as an alternative one-pot procedure for *in situ* development of nano-objects with tunable morphologies at high solid concentrations (typically 10−30% w/w).[7−10] During block copolymer PISA, direct nanoparticle fabrication is achieved as a solvent-soluble corona-forming block is chain extended using specific solvent-miscible (dispersion PISA) or solvent-immiscible (emulsion PISA) monomers that form a second, insoluble core block.[11]

To date, the majority of literature reports on PISA has been dominated by reversible-deactivation radical polymerization (RDRP) techniques, mainly involving atom transfer radical polymerization (ATRP)[12,13] and reversible addition−fragmentation chain-transfer (RAFT) polymerization,[14−17] in both aqueous and organic media. However, PISA mediated by ring-opening metathesis polymerization (ROMPISA) has recently emerged as a nonradical technology for block copolymer self-assembly. This growing research interest is facilitated by the robust nature of commercially available Ru-based catalysts, fast polymerization kinetics, and the ability to conduct polymerizations under air at ambient temperature in either organic or aqueous milieu.[18−20]

Since ROMPISA is a newly established concept, a very limited number of monomers that are able to undergo the described solubility transition upon polymerization to achieve *in situ* self-assembly are known, especially in dispersed aqueous media. In particular, a few monomers that undergo ROMPISA in organic solvent or under aqueous emulsion conditions have been reported thus far,[21−25] while Gianneschi's group introduced a quaternary amine-based phenyl norbornene dicarboximide monomer as the core-forming block in aqueous dispersion ROMPISA.[26,27] In addition, *exo*-5-norbornenecarboxylic acid and a di(oligo(ethylene glycol))-based norbornene monomer have been reported by our group for use in aqueous dispersion ROMPISA *via* a water-soluble macroinitiator approach.[28] Hence, opportunities exist for identification of new core-forming ROMPISA monomers.

Recently, our group reported an *in silico* method that allows for prediction of monomers that could be used either as

Received: February 16, 2019
Accepted: March 19, 2019
Published: April 3, 2019

DOI: 10.1021/acsmacrolett.9b00117
ACS Macro Lett. 2019, 8, 466−472

corona- or core-forming blocks in aqueous RAFT-mediated PISA through oligomer hydrophobicity evaluation, as well as for prediction of morphologies for PISA systems implemented with different monomer chemistries.[29] Herein, this process is applied to predict a set of norbornene monomers with various functionalities for use in aqueous ROMPISA. Diblock copolymer nano-objects were successfully developed *via* one-pot ROMPISA using the predicted monomers as core-forming blocks and the same hydrophilic stabilizer block as the macroinitiator, following our recently reported procedure for controlled ROMP in aqueous media.[28] The order of resulting morphologies increased upon respective degree of polymerization (DP) and relative hydrophobicity increase, while structure−property relationships were also identified based on our monomer design.

The predictive methodology followed for identifying whether a monomer will be able to undergo aqueous ROMPISA is based on *in silico* determination of hydrophobicity for corresponding oligomeric models by calculating octanol−water partition coefficients ($Log P_{oct}$). This analysis has been well-established for small molecules, while transitioning to larger polymer molecules benefits from normalization of $Log P_{oct}$ values by solvent-accessible surface area (SA) to minimize molecular weight and end-group discrepancies.[30−32] Olefin end-groups were chosen for the oligomer models in all calculations for simplicity. While end-group hydrophobicity contributes to the $Log P_{oct}$/SA value for short oligomers (i.e., DP < 10), the influence of end-groups becomes negligible as DP increases.[30] Positive $Log P_{oct}$/SA values correspond to hydrophobic polymers that primarily partition into the octanol phase and as such can be used in core-forming blocks during ROMPISA in aqueous media. On the contrary, water-soluble polymers possess negative $Log P_{oct}$/SA values, indicating their ability to be used in corona-forming blocks. The importance of the sign of $Log P_{oct}$/SA can be understood by comparing homopolymer solubility; for example, homopolymers synthesized using **M8** or **M9** were completely insoluble in water, whereas **P(M10)** could be readily dissolved.

Using the described predictive methodology (see Supporting Information for detailed description), $Log P_{oct}$/SA values of ROMP oligomers ranging from 3-mers to 12-mers were calculated for a series of norbornene-based monomers bearing a wide range of functional groups. A correlation between oligomer $Log P_{oct}$/SA and monomer $Log P_{oct}$ was also identified, giving insight into the water solubility of their respective homopolymers (Figure S1). Monomers used in our study were mainly selected based on their relatively facile one- or two-step syntheses from commercially available precursor compounds. We also hypothesized that hydrophobicity trends for this wide range of monomers with different anchor or terminal functional groups would elicit important structure−property relationships. For comparison, $Log P_{oct}$/SA analysis of previously reported monomers used in aqueous ROMPISA (**MX** = **M1**, **M4**, **M7**, and **M11**) was also carried out.[26,28] The hydrophobicity evaluation results for $\mathbf{P(MX)}_n$ (**MX** = **M1**−**M11**) ROMP oligomers as a function of increasing chain length along with their corresponding monomer structures are shown in Figure 1.

A plethora of studied monomers (**M1**−**M9**) were predicted to be suitable for core-forming blocks in aqueous ROMPISA as their respective oligomers possess positive $Log P_{oct}$/SA values across all chain lengths. In general, the imide-based oligomers (**M4**−**M6** and **M9**) were less hydrophobic than the ester-/amide-based ones (**M1**−**M3** and **M8**), while multiple polar functional groups or charges were required to achieve negative oligomer $Log P_{oct}$/SA values suitable for hydrophilic corona-forming blocks (**M10** and **M11**).

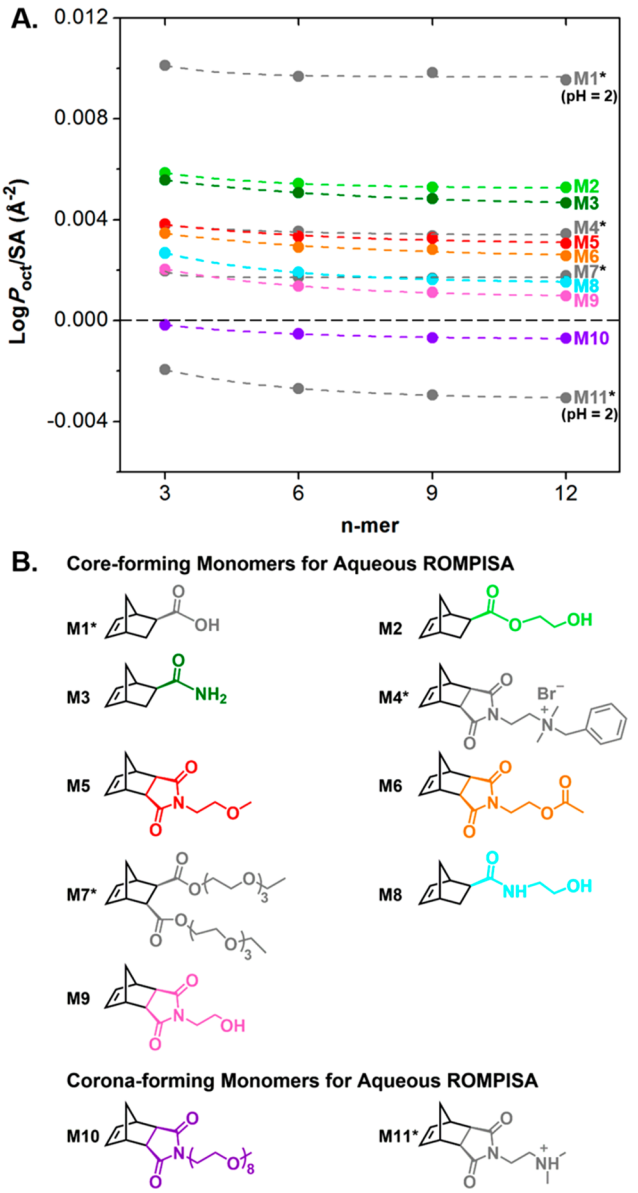

Figure 1. (A) Evolution of $\mathbf{P(MX)}_n$ (**MX** = **M1**−**M11**) ROMP oligomer hydrophobicity as a function of the length of the oligomer. $Log P_{oct}$ values (ALogP98 method) were calculated using an atom-based approach and normalized by solvent-accessible surface area (SA) using Materials Studio 2018. The $Log P_{oct}$/SA > 0 region corresponds to core-forming blocks, while the $Log P_{oct}$/SA < 0 region corresponds to corona-forming blocks. (B) Core- and corona-forming norbornene-based monomer structures for aqueous ROMPISA. Monomers marked with an asterisk (*) have been reported in the literature.

To correlate computational hydrophobicity trends with experimental results, two criteria were envisioned for monomer design. First, the ease of monomer synthesis was considered. Monomers **M2**, **M3**, **M5**, **M6**, and **M8**−**M11** were synthesized following simple imide formation or esterification/amidation procedures (see Supporting Information for experimental details). Second, the solubility of prepared monomers in aqueous media was of major significance. Importantly, the

DOI: 10.1021/acsmacrolett.9b00117
ACS Macro Lett. 2019, 8, 466−472

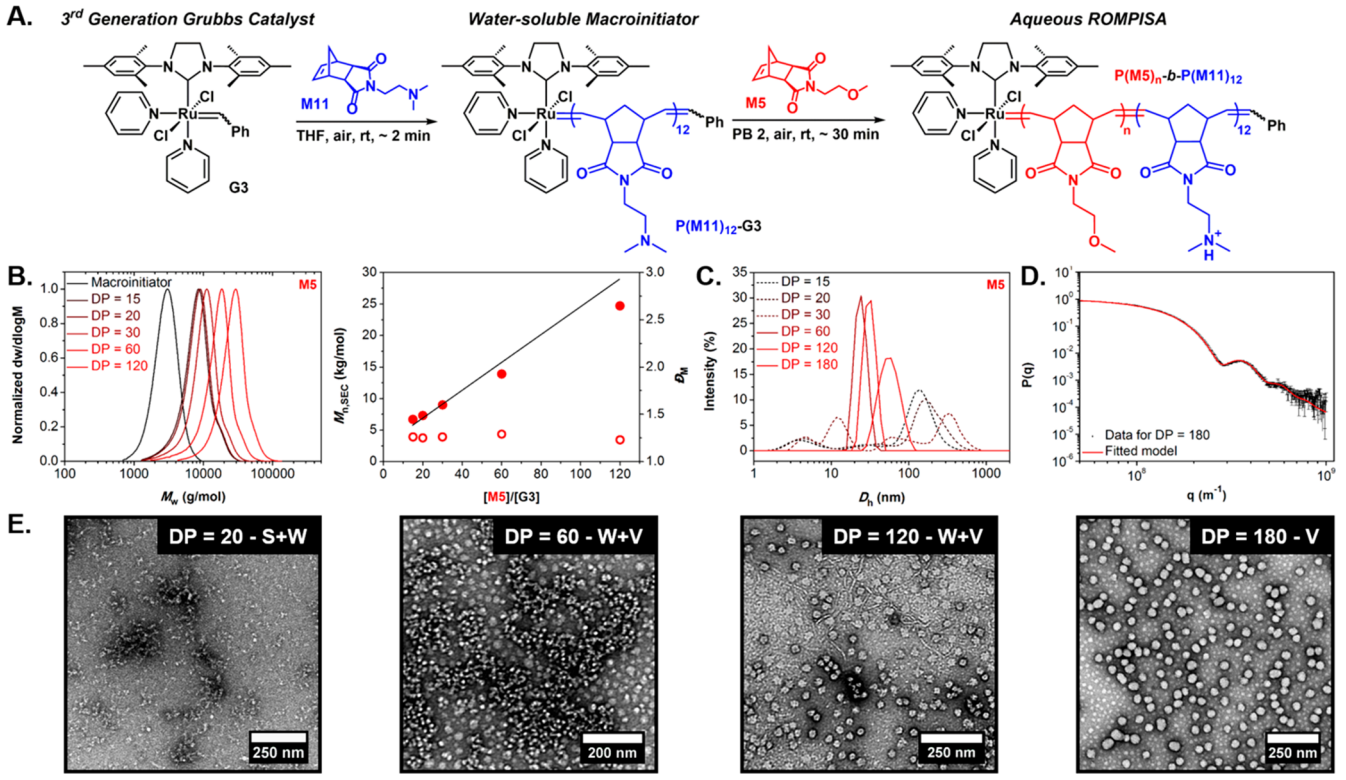

Figure 2. (A) Schematic representation of the synthetic route followed for the development of $\mathbf{P(M11)_{12}}$-*b*-$\mathbf{P(M5)_n}$ (n = 15, 20, 30, 60, 120, and 180) diblock copolymer nano-objects *via* aqueous ROMPISA using a water-soluble $\mathbf{P(M11)_{12}}$ macroinitiator. (B) Normalized SEC RI molecular weight distributions, and evolution of M_n (filled circles) and $Đ_M$ (empty circles) values calculated from SEC analysis with increasing targeted $DP_{P(M5)}$ for $\mathbf{P(M11)_{12}}$-*b*-$\mathbf{P(M5)_n}$ diblock copolymers. The solid line represents expected M_n values calculated using the monomer feed ratio, assuming full monomer conversion. M_n and $Đ_M$ values were calculated from PS standards using THF + 2% v/v NEt_3 as the eluent. (C) Intensity weighted size distributions obtained by DLS for $\mathbf{P(M11)_{12}}$-*b*-$\mathbf{P(M5)_n}$ diblock copolymer nano-objects. (D) Fitted model to SAXS data recorded for $\mathbf{P(M11)_{12}}$-*b*-$\mathbf{P(M5)_{180}}$. (E) Representative dry-state TEM images of $\mathbf{P(M11)_{12}}$-*b*-$\mathbf{P(M5)_n}$ diblock copolymer nano-objects, stained with 1 wt% uranyl acetate (UA) solution.

majority of monomers in Figure 1B were found to be water-miscible at [**MX**] = 1 wt%, underlying their ability to be used in aqueous dispersion ROMPISA. Based on these findings, we chose to evaluate diblock copolymer ROMPISA using monomers **M2**, **M3**, **M5**, **M6**, **M8**, and **M9** as core-forming blocks and **M11** as the corona-forming block following our reported methodology to conduct well-controlled, open-to-air ROMP in aqueous media using a macroinitiator approach.[28]

A **P(M11)** macroinitiator was first synthesized *via* ROMP, under air, in a water-miscible organic solvent (i.e., THF) using the commercially available third-generation Grubbs catalyst (G3) ($DP_{P(M11)}$ = 12, $M_{n,NMR}$ = 2.8 kDa, $M_{n,SEC}$ = 2.6 kDa, $Đ_M$ = 1.17, Table S1). An aliquot of the resulting macroinitiator in THF was then added to a solution of a second core-forming monomer (**MX** = **M2**, **M3**, **M5**, **M6**, **M8**, or **M9**) in acidic phosphate buffer (pH = 2, PB 2) (PB/THF = 9:1, [**MX**] = 1 wt%), where ionization of the pendant tertiary amine groups of **P(M11)** occurred yielding the charged hydrophilic stabilizer block (see Figure S2 for pH-dependent solubility of **P(M11)** oligomers). The presence of acid also promoted pyridine ligand dissociation to generate the active form of the G3 catalyst. Chain extensions for the development of $\mathbf{P(M11)_{12}}$-*b*-$\mathbf{P(MX)_n}$ diblock copolymer nano-objects *via* ROMPISA targeting increasing DP of **P(MX)** were fast and typically completed within a 2−30 min time scale, depending on the monomer. As a representative example, the obtained characterization results from aqueous ROMPISA of **M5** are given in detail in Figure 2.

Based on the described synthetic route, a series of aqueous ROMPISA reactions using **M5** were conducted over a range of DPs of **P(M5)** core-forming blocks by varying the initial [**M5**]/[G3] feed ratio, using a water-soluble $\mathbf{P(M11)_{12}}$ macroinitiator (Figure 2A). A gradual turbidity increase was noticed for polymerization solutions with increasing $DP_{P(M5)}$, indicating the onset of particle micellization. Quantitative monomer conversions (>99%) were achieved in all cases after approximately 30 min, as determined by ^{1}H NMR spectroscopic analysis in methanol-d_4 of the crude samples. SEC analysis of $\mathbf{P(M11)_{12}}$-*b*-$\mathbf{P(M5)_n}$ diblock copolymers, using THF + 2% v/v triethylamine (NEt_3) as the eluent, revealed the well-controlled character of the aqueous ROMPISA process using **M5**. Specifically, symmetrical, monomodal molecular weight distributions were observed, shifting linearly toward higher molecular weight (M_n) values upon increasing the DP of **P(M5)**. Calculated M_n values agreed well with theoretically expected values, while dispersity ($Đ_M$) values remained low ($Đ_M$ < 1.30) throughout (Figure 2B and Table S4).

DLS analysis of $\mathbf{P(M11)_{12}}$-*b*-$\mathbf{P(M5)_n}$ ROMPISA solutions revealed the formation of particles with multiple populations and high polydispersity (PD) values for the lower DPs of **P(M5)**, suggesting the development of worm-like micelles or nano-objects with mixed morphologies, while single particle populations with low PD were observed for $DP_{P(M5)} \geq 60$

DOI: 10.1021/acsmacrolett.9b00117
ACS Macro Lett. 2019, 8, 466−472

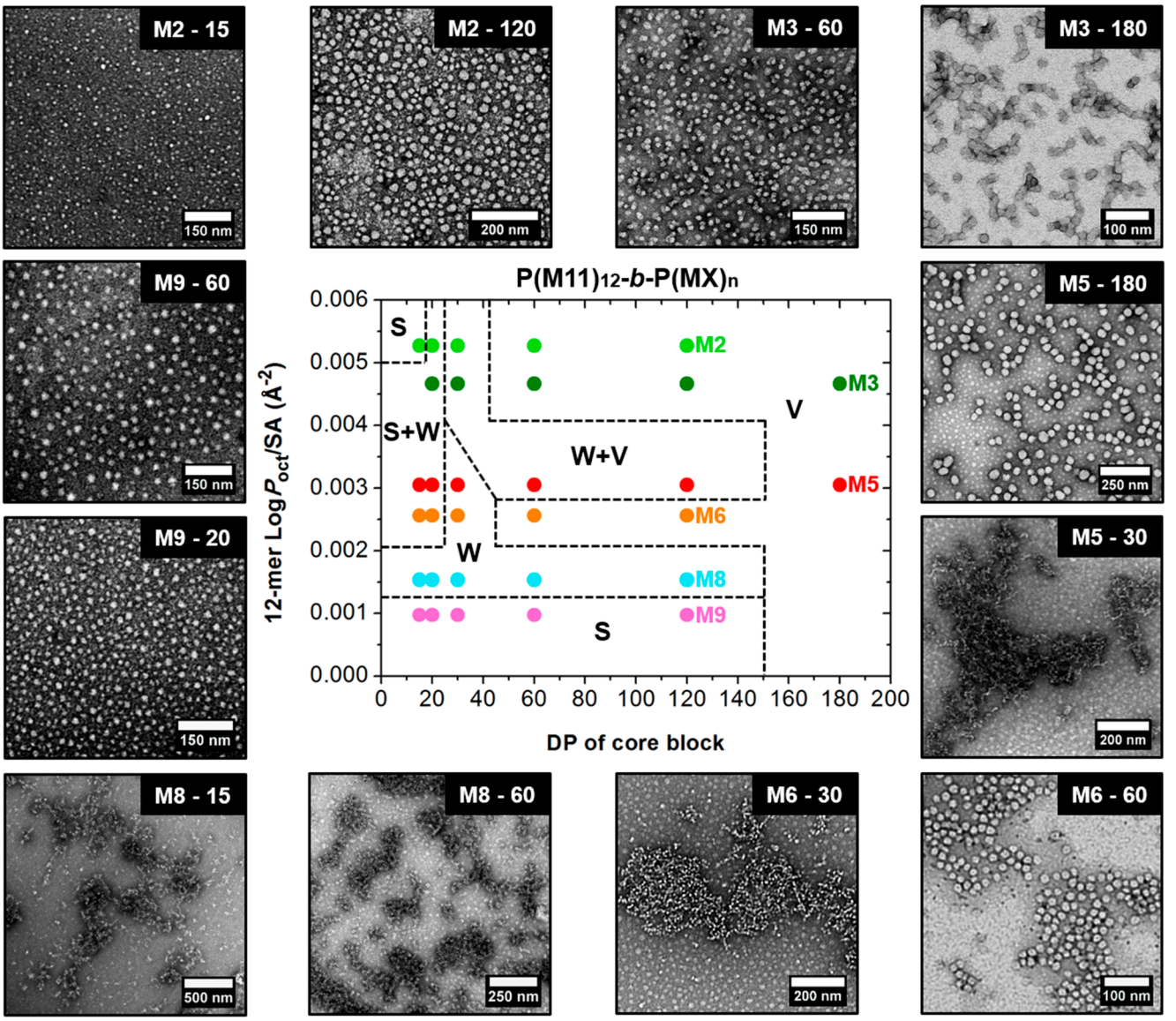

Figure 3. Detailed phase diagram for $\mathbf{P(M11)_{12}}$-*b*-$\mathbf{P(MX)_n}$ (**MX** = **M2**, **M3**, **M5**, **M6**, **M8**, and **M9**) diblock copolymer nano-objects prepared *via* aqueous ROMPISA by varying the DP of the **P(MX)** core block as a function of corresponding 12-mer LogP_{oct}/SA values, along with representative dry-state TEM images of different formulations stained with 1 wt% uranyl acetate (UA) solution (Key: S, spherical micelles; W, worm-like micelles; V, vesicles).

indicating the formation of uniform assemblies (Figure 2C and Table S12). Dry-state and cryo-TEM imaging further supported the DLS findings and showed an evolution in morphology from spheres and short worms ($DP_{P(M5)} \leq 30$) to mixed morphologies of worms and vesicles ($60 \leq DP_{P(M5)} \leq 120$) and finally to single-phase vesicles of uniform size ($DP_{P(M5)} = 180$) as the DP of the core-forming block increased (Figures 2E, S28, and S32). The observed pure worm ($DP_{P(M5)} = 30$) and vesicle ($DP_{P(M5)} = 180$) morphologies were further investigated by small-angle X-ray scattering (SAXS) analysis (Figures 2D and S33). For $DP_{P(M5)} = 180$, the scattering data were consistent with a parsimonious model for scattering by spherical particles, and fitted values to describe the particle size distribution were consistent with TEM imaging observations. However, the existence of an inner aqueous compartment could not be verified from SAXS data, as parameters within the parsimonious model could potentially mask its existence, especially if the size of this compartment is on the order of variability in particle size (i.e., a few nanometers). Notably, our theoretical model correctly predicted that the rest of the monomers with positive oligomer LogP_{oct}/SA values (**MX** = **M2**, **M3**, **M6**, **M8**, and **M9**) could also be used as hydrophobic core blocks during ROMPISA in aqueous media. Similar analysis with comparable results was performed for $\mathbf{P(M11)_{12}}$-*b*-$\mathbf{P(MX)_n}$ diblock copolymer nano-objects prepared *via* aqueous ROMPISA using the other predicted core-forming monomers (see Supporting Information for characterization results). In contrast, predicted monomer **M10** with negative oligomer LogP_{oct}/SA values could be successfully utilized as the corona-forming block since it only formed water-soluble polymers, while its ability to be chain-extended in a controlled manner under the same aqueous ROMP conditions was further confirmed (Figure S24 and Tables S8–S9).

According to our previous report on predicting new monomers for use in aqueous RAFT-mediated PISA, we applied the LogP_{oct}/SA analysis to reliably predict ROMPISA

DOI: 10.1021/acsmacrolett.9b00117
ACS Macro Lett. 2019, 8, 466–472

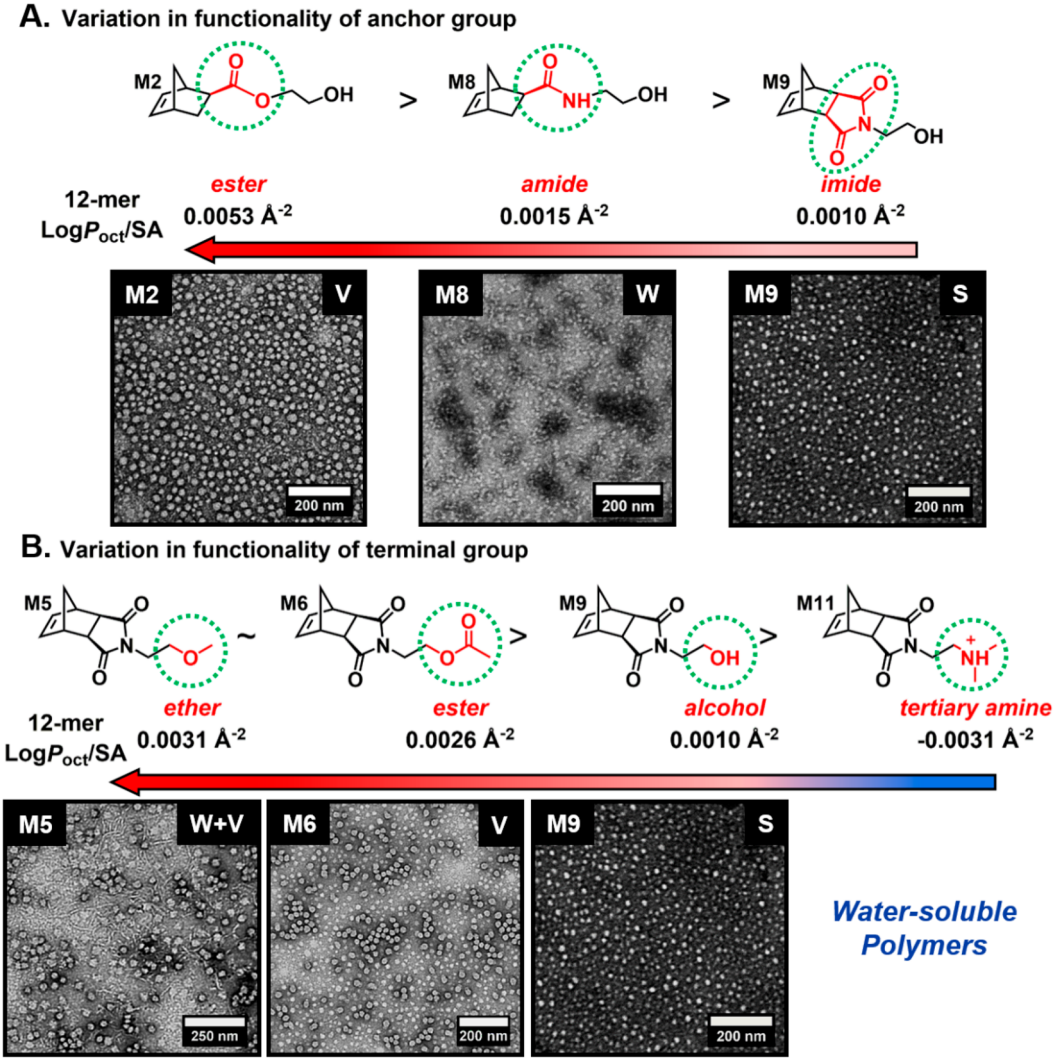

Figure 4. Hydrophobicity trends for different anchor groups (A) and different terminal groups (B) for norbornene-based monomers involved in aqueous ROMPISA based on LogP_{oct}/SA analysis from Materials Studio 2018 and corresponding dry-state TEM images for $\mathbf{P(M11)}_{12}$-*b*-$\mathbf{P(MX)}_n$ diblock copolymer nano-objects at $DP_{P(MX)}$ = 120 showing higher-order morphologies upon increasing polymer hydrophobicity.

morphologies.[29] Herein, contrary to traditional phase diagrams for PISA formulations that show morphology progression as a function of increasing DP and solid content, a phase diagram for $\mathbf{P(M11)}_{12}$-*b*-$\mathbf{P(MX)}_n$ diblock copolymer nano-objects was constructed based on the relative hydrophobicity of $\mathbf{P(MX)}_n$ homopolymers. To assist comparisons across the phase diagram, all ROMPISA reactions were carried out at the same solid concentration (Figure 3).

We hypothesized that nano-object morphology would evolve toward higher-order structures with increasing DP of the core block and LogP_{oct}/SA value for the same oligomer length (i.e., up and to the right of the phase diagram). Confirming this hypothesis, small spherical micelles were generally observed for low hydrophobicity values and low DPs of **P(MX)**, while worm-like micelles or mixed morphologies mostly occupied the middle region of the phase diagram. Finally, TEM imaging revealed the formation of vesicular structures for high DPs and high 12-mer LogP_{oct}/SA values (Figures S26−S32). The vesicle morphologies were confirmed to contain inner compartments by cryo-TEM. It is worth mentioning that some polymers did not conform perfectly to this trend. This discrepancy did not arise from differences in polymer T_g values, as confirmed by microDSC (Figure S23). Instead, morphological exceptions could originate from differences in polymerization kinetics of the various monomers. For instance, imide norbornene monomers are known to polymerize more slowly compared to their ester or amide counterparts, as could be the case with **M5**.[33−35] As such, the morphologies obtained using **M2** and **M3** could be kinetically trapped and may not represent equilibrium structures. Despite that, there is still an overall trend of higher-order structures obtained as LogP_{oct}/SA increases for a certain DP of **P(MX)** that agrees well with our predictive methodology.

Based on our sophisticated monomer design, the investigation of potential hydrophobicity trends for ROMPISA monomers which differ solely in terms of anchor or terminal group functionality has yielded meaningful insight into structure−property relationships. First, the variation in functionality of the anchor group for monomers with the same terminal alcohol group was considered (Figure 4A). LogP_{oct}/SA analysis for ROMP oligomers showed that the ester anchor group of **M2** was more hydrophobic than the amide linkage of **M8**, which in turn was more hydrophobic than the respective imide group of **M9**. Aqueous ROMPISA

DOI: 10.1021/acsmacrolett.9b00117
ACS Macro Lett. 2019, 8, 466−472

reactions for the synthesis of $\mathbf{P(M11)_{12}}$-*b*-$\mathbf{P(MX)_n}$ diblock copolymer nano-objects using **MX** = **M2**, **M8**, and **M9** were conducted targeting the same DP of the core-froming block ($DP_{P(MX)}$ = 120) to confirm this trend. Prepared diblock copolymers had similar length, although the morphologies of obtained PISA formulations differed significantly and trended based on polymer hydrophobicity. For the most hydrophobic monomer, **M2**, spherical vesicles were formed at DP = 120, while networks of worm-like micelles were developed for less hydrophobic **M8** and small spherical micelles for **M9** at the same DP.

Next, hydrophobicity trends for monomers with the same imide anchor group and different terminal functional groups were studied (Figure 4B). In particular, our model suggested that the ether terminal group of **M5** was more hydrophobic than the methyl ester group of **M6** and the respective alcohol group of **M9**, while the protonated tertiary amine group of **M11** was the most hydrophilic, forming water-soluble polymers regardless of block length. Indeed, for $\mathbf{P(M11)_{12}}$-*b*-$\mathbf{P(MX)_n}$ nano-objects using **MX** = **M5**, **M6**, and **M9** with comparable block lengths, higher-order morphologies were obtained with increasing magnitude of 12-mer $\mathrm{Log}P_{oct}$/SA values at the same DP of **P(MX)**.

To conclude, we report an *in silico* predictive methodology based on oligomer hydrophobicity calculations for successful identification of new monomers with a wide range of functionalities for use in aqueous ROMPISA as corona- or core-forming blocks. Upon ROMPISA using the predicted monomers, common nano-object morphologies were accessed that were found to evolve toward higher-order structures with increasing DP and oligomer hydrophobicity values. Importantly, valuable oligomer hydrophobicity trends were identified based on different monomer structures that allow for reliable morphology prediction. Overall, our study could further expand the field of PISA beyond RDRP techniques and pave the way for discovering new monomers that undergo ROMPISA.

■ ASSOCIATED CONTENT

Supporting Information

The Supporting Information is available free of charge on the ACS Publications website at DOI: 10.1021/acsmacrolett.9b00117.

Materials and characterization techniques, oligomer hydrophobicity evaluation details, synthetic procedures, additional SEC data of diblock copolymers, additional microDSC, DLS, and SAXS data, and dry-state and cryo-TEM images of nano-objects (PDF)

■ AUTHOR INFORMATION

Corresponding Authors

*E-mail: rtm11@psu.edu (R.T.M.).
*E-mail: r.oreilly@bham.ac.uk (R.K.O.R.).

ORCID

Spyridon Varlas: 0000-0002-4171-7572
Robert T. Mathers: 0000-0002-0503-4571
Rachel K. O'Reilly: 0000-0002-1043-7172

Author Contributions

The manuscript was written through contributions of all authors. All authors have given approval to the final version of the manuscript.

Notes

The authors declare no competing financial interest.

■ ACKNOWLEDGMENTS

This work was supported by the ERC (grant number 615142), EPSRC, and the University of Birmingham. Mr. Z. Coe (University of Birmingham) is thanked for microDSC assistance, and Dr. S. Bakker (University of Warwick) is thanked for cryo-TEM assistance. Advanced BioImaging Research Technology Platform, BBSRC ALERT14 award BB/M01228X/1, is thanked for supporting cryo-TEM characterization. Steven Huband at the University of Warwick X-ray Diffraction Research Technology Platform is thanked for assisting with SAXS measurements.

■ REFERENCES

(1) Blanazs, A.; Armes, S. P.; Ryan, A. J. Self-Assembled Block Copolymer Aggregates: From Micelles to Vesicles and their Biological Applications. *Macromol. Rapid Commun.* **2009**, *30*, 267−277.

(2) Mai, Y.; Eisenberg, A. Self-assembly of block copolymers. *Chem. Soc. Rev.* **2012**, *41*, 5969−5985.

(3) Rodríguez-Hernández, J.; Chécot, F.; Gnanou, Y.; Lecommandoux, S. Toward 'smart' nano-objects by self-assembly of block copolymers in solution. *Prog. Polym. Sci.* **2005**, *30*, 691−724.

(4) Brendel, J. C.; Schacher, F. H. Block Copolymer Self-Assembly in Solution—Quo Vadis? *Chem. - Asian J.* **2018**, *13*, 230−239.

(5) Patterson, J. P.; Robin, M. P.; Chassenieux, C.; Colombani, O.; O'Reilly, R. K. The analysis of solution self-assembled polymeric nanomaterials. *Chem. Soc. Rev.* **2014**, *43*, 2412−2425.

(6) Charleux, B.; Delaittre, G.; Rieger, J.; D'Agosto, F. Polymerization-Induced Self-Assembly: From Soluble Macromolecules to Block Copolymer Nano-Objects in One Step. *Macromolecules* **2012**, *45*, 6753−6765.

(7) Warren, N. J.; Armes, S. P. Polymerization-Induced Self-Assembly of Block Copolymer Nano-objects via RAFT Aqueous Dispersion Polymerization. *J. Am. Chem. Soc.* **2014**, *136*, 10174−10185.

(8) Yeow, J.; Boyer, C. Photoinitiated Polymerization-Induced Self-Assembly (Photo-PISA): New Insights and Opportunities. *Adv. Sci.* **2017**, *4*, 1700137.

(9) Wang, X.; An, Z. New Insights into RAFT Dispersion Polymerization-Induced Self-Assembly: From Monomer Library, Morphological Control, and Stability to Driving Forces. *Macromol. Rapid Commun.* **2019**, *40*, 1800325.

(10) Liu, X.; Sun, M.; Sun, J.; Hu, J.; Wang, Z.; Guo, J.; Gao, W. Polymerization Induced Self-Assembly of a Site-Specific Interferon α-Block Copolymer Conjugate into Micelles with Remarkably Enhanced Pharmacology. *J. Am. Chem. Soc.* **2018**, *140*, 10435−10438.

(11) Canning, S. L.; Smith, G. N.; Armes, S. P. A Critical Appraisal of RAFT-Mediated Polymerization-Induced Self-Assembly. *Macromolecules* **2016**, *49*, 1985−2001.

(12) Wang, G.; Schmitt, M.; Wang, Z.; Lee, B.; Pan, X.; Fu, L.; Yan, J.; Li, S.; Xie, G.; Bockstaller, M. R.; Matyjaszewski, K. Polymerization-Induced Self-Assembly (PISA) Using ICAR ATRP at Low Catalyst Concentration. *Macromolecules* **2016**, *49*, 8605−8615.

(13) Wang, J.; Wu, Z.; Wang, G.; Matyjaszewski, K. In Situ Crosslinking of Nanoparticles in Polymerization-Induced Self-Assembly via ARGET ATRP of Glycidyl Methacrylate. *Macromol. Rapid Commun.* **2019**, *40*, 1800332.

(14) Warren, N. J.; Mykhaylyk, O. O.; Mahmood, D.; Ryan, A. J.; Armes, S. P. RAFT aqueous dispersion polymerization yields poly(ethylene glycol)-based diblock copolymer nano-objects with predictable single phase morphologies. *J. Am. Chem. Soc.* **2014**, *136*, 1023−1033.

(15) Ng, G.; Yeow, J.; Xu, J.; Boyer, C. Application of oxygen tolerant PET-RAFT to polymerization-induced self-assembly. *Polym. Chem.* **2017**, *8*, 2841−2851.

DOI: 10.1021/acsmacrolett.9b00117
ACS Macro Lett. 2019, 8, 466−472

(16) Blackman, L. D.; Varlas, S.; Arno, M. C.; Fayter, A.; Gibson, M. I.; O'Reilly, R. K. Permeable Protein-Loaded Polymersome Cascade Nanoreactors by Polymerization-Induced Self-Assembly. *ACS Macro Lett.* **2017**, *6*, 1263−1267.
(17) Varlas, S.; Blackman, L. D.; Findlay, H. E.; Reading, E.; Booth, P. J.; Gibson, M. I.; O'Reilly, R. K. Photoinitiated Polymerization-Induced Self-Assembly in the Presence of Surfactants Enables Membrane Protein Incorporation into Vesicles. *Macromolecules* **2018**, *51*, 6190−6201.
(18) Bielawski, C. W.; Grubbs, R. H. Highly Efficient Ring-Opening Metathesis Polymerization (ROMP) Using New Ruthenium Catalysts Containing N-Heterocyclic Carbene Ligands. *Angew. Chem., Int. Ed.* **2000**, *39*, 2903−2906.
(19) Sutthasupa, S.; Shiotsuki, M.; Sanda, F. Recent advances in ring-opening metathesis polymerization, and application to synthesis of functional materials. *Polym. J.* **2010**, *42*, 905.
(20) Radzinski, S. C.; Foster, J. C.; Matson, J. B. Synthesis of bottlebrush polymers via transfer-to and grafting-through approaches using a RAFT chain transfer agent with a ROMP-active Z-group. *Polym. Chem.* **2015**, *6*, 5643−5652.
(21) Zhang, L.; Song, C.; Yu, J.; Yang, D.; Xie, M. One-pot synthesis of polymeric nanoparticle by ring-opening metathesis polymerization. *J. Polym. Sci., Part A: Polym. Chem.* **2010**, *48*, 5231−5238.
(22) Liu, J.; Liao, Y.; He, X.; Yu, J.; Ding, L.; Xie, M. Facile One-Pot Approach for Preparing Functionalized Polymeric Nanoparticles via ROMP. *Macromol. Chem. Phys.* **2011**, *212*, 55−63.
(23) Yoon, K.-Y.; Lee, I.-H.; Kim, K. O.; Jang, J.; Lee, E.; Choi, T.-L. One-Pot in Situ Fabrication of Stable Nanocaterpillars Directly from Polyacetylene Diblock Copolymers Synthesized by Mild Ring-Opening Metathesis Polymerization. *J. Am. Chem. Soc.* **2012**, *134*, 14291−14294.
(24) Wright, D. B.; Touve, M. A.; Adamiak, L.; Gianneschi, N. C. ROMPISA: Ring-Opening Metathesis Polymerization-Induced Self-Assembly. *ACS Macro Lett.* **2017**, *6*, 925−929.
(25) Torres-Rocha, O. L.; Wu, X.; Zhu, C.; Crudden, C. M.; Cunningham, M. F. Polymerization-Induced Self-Assembly (PISA) of 1,5-Cyclooctadiene Using Ring Opening Metathesis Polymerization. *Macromol. Rapid Commun.* **2019**, *40*, 1800326.
(26) Wright, D. B.; Touve, M. A.; Thompson, M. P.; Gianneschi, N. C. Aqueous-Phase Ring-Opening Metathesis Polymerization-Induced Self-Assembly. *ACS Macro Lett.* **2018**, *7*, 401−405.
(27) Wright, D. B.; Thompson, M. P.; Touve, M. A.; Carlini, A. S.; Gianneschi, N. C. Enzyme-Responsive Polymer Nanoparticles via Ring-Opening Metathesis Polymerization-Induced Self-Assembly. *Macromol. Rapid Commun.* **2019**, *40*, 1800467.
(28) Foster, J. C.; Varlas, S.; Blackman, L. D.; Arkinstall, L. A.; O'Reilly, R. K. Ring-Opening Metathesis Polymerization in Aqueous Media Using a Macroinitiator Approach. *Angew. Chem., Int. Ed.* **2018**, *57*, 10672−10676.
(29) Foster, J. C.; Varlas, S.; Couturaud, B.; Jones, J. R.; Keogh, R.; Mathers, R. T.; O'Reilly, R. K. Predicting Monomers for Use in Polymerization-Induced Self-Assembly. *Angew. Chem., Int. Ed.* **2018**, *57*, 15733−15737.
(30) Magenau, A. J. D.; Richards, J. A.; Pasquinelli, M. A.; Savin, D. A.; Mathers, R. T. Systematic Insights from Medicinal Chemistry To Discern the Nature of Polymer Hydrophobicity. *Macromolecules* **2015**, *48*, 7230−7236.
(31) Yildirim, E.; Dakshinamoorthy, D.; Peretic, M. J.; Pasquinelli, M. A.; Mathers, R. T. Synthetic Design of Polyester Electrolytes Guided by Hydrophobicity Calculations. *Macromolecules* **2016**, *49*, 7868−7876.
(32) Dharmaratne, N. U.; Jouaneh, T. M. M.; Kiesewetter, M. K.; Mathers, R. T. Quantitative Measurements of Polymer Hydrophobicity Based on Functional Group Identity and Oligomer Length. *Macromolecules* **2018**, *51*, 8461−8468.
(33) Radzinski, S. C.; Foster, J. C.; Chapleski, R. C.; Troya, D.; Matson, J. B. Bottlebrush Polymer Synthesis by Ring-Opening Metathesis Polymerization: The Significance of the Anchor Group. *J. Am. Chem. Soc.* **2016**, *138*, 6998−7004.
(34) Slugovc, C.; Demel, S.; Riegler, S.; Hobisch, J.; Stelzer, F. The Resting State Makes the Difference: The Influence of the Anchor Group in the ROMP of Norbornene Derivatives. *Macromol. Rapid Commun.* **2004**, *25*, 475−480.
(35) Chang, A. B.; Lin, T.-P.; Thompson, N. B.; Luo, S.-X.; Liberman-Martin, A. L.; Chen, H.-Y.; Lee, B.; Grubbs, R. H. Design, Synthesis, and Self-Assembly of Polymers with Tailored Graft Distributions. *J. Am. Chem. Soc.* **2017**, *139*, 17683−17693.

DOI: 10.1021/acsmacrolett.9b00117
ACS Macro Lett. 2019, 8, 466−472